Optical Engineering

SPIEDigitalLibrary.org/oe

Potentials of acousto-optical spectrum analysis on a basis of a novel algorithm of the collinear wave heterodyning in a large-aperture KRS–5 crystalline cell

Alexandre S. Shcherbakov
Jewgenij Maximov
Alexej M. Bliznetsov
Karla J. Sanchez Perez

Potentials of acousto-optical spectrum analysis on a basis of a novel algorithm of the collinear wave heterodyning in a large-aperture KRS–5 crystalline cell

Alexandre S. Shcherbakov
National Institute for Astrophysics, Optics, and Electronics
Department of Optics
A.P. 51 y 216
Calle Luis Enrique Erro 1
Tonantzintla, Puebla 72000, Mexico

Jewgenij Maximov
Molecular Technology GmbH
Rudower Chaussee 29-31
Berlin, 12489, Germany

Alexej M. Bliznetsov
Saint-Petersburg State Polytechnic University
Radio-Physics Department
Polytechnicheskaya Street 29
St. Petersburg, 195251, Russian Federation

Karla J. Sanchez Perez
National Institute for Astrophysics, Optics, and Electronics
Department of Optics
Calle Luis Enrique Erro 1
Tonantzintla, Puebla 72000, Mexico
E-mail: kjaneth279@inaoep.mx

Abstract. The technique under proposal for a precise spectrum analysis within an algorithm of the collinear wave heterodyning implies a two-stage integrated processing, namely, the wave heterodyning of a signal in a square-law nonlinear medium and then the optical processing in the same solid state cell. The technical advantage of this approach lies in providing a direct multichannel parallel processing of ultra-high-frequency radio-wave signals with essentially improved frequency resolution. This technique imposes specific requirements on the cell's material. We focus our attention on the solid solutions of thallium chalcogenides and take the TlBr–TlI (thallium bromine–thallium iodine) solution, which forms KRS–5 cubic-symmetry crystals with the mass-ratio 58% of TlBr to 42% of TlI. Analysis shows that the acousto-optical cell made of a KRS–5 crystal oriented along the [111]-axis and the corresponding longitudinal elastic mode for producing the dynamic diffractive grating can be exploited. With the acoustic velocity of about 1.92×10^5 cm/s and attenuation of $\sim$10 dB/(cm GHz^2), a similar cell is capable of providing an optical aperture of $\sim$5.0 cm and one of the highest figures of acousto-optical merit in solid states in the visible range. Such a cell is rather desirable for the application to direct 5000-channel parallel spectrum analysis with an improved up to 10^{-5} relative frequency resolution. [DOI: 10.1117/1.3549892]

Subject terms: precise spectrum analysis; codirectional collinear wave heterodyning; acoustooptical interaction in crystals.

Paper 100724R received Sep. 10, 2010; revised manuscript received Jan. 7, 2011; accepted for publication Jan. 11, 2011; published online Mar. 25, 2011.

1 Introduction

A notable portion of modern technical achievements in a high-bit-rate optical data processing is directly connected with utilizing such nonlinear phenomena as, for example, wave mixing, various cross- and self-actions, etc.[1,2] Recently, a two-cascade processing based on a three-wave interaction between coherent waves of different natures (optical and nonoptical) had been successfully realized.[3] Then, in a line with this, potential performances connected with using a collinear wave mixing in the specific case of a medium without any group-velocity dispersion while with strongly dispersive losses had been demonstrated.[4,5] The proposed approach makes it possible to provide an effective wave heterodyning, when the beneficial data in signal is converted from a relatively high-frequency carrier wave to a difference frequency wave. Because of rather strong square-law dispersion of linear acoustic losses, heterodyning leads to increasing the characteristic length and time of propagation (they both are associated with a clear optical aperture) for the converted signal in that medium and to significantly improving the accuracy of signal processing, as follows from the uncertainty principle in quantum mechanics.[6] In this context, we consider an opportunity for real-time scale optical analysis of frequency spectra, belonging to analog ultrahigh-frequency radio-wave signals, with significantly improved frequency resolution. This consideration is based on a two-cascade processing, i.e., on exploiting a pair of different wave processes, one after the other, sequentially in a single crystalline cell, which includes the piezoelectric transducer, converting the inputting electronic signals into gigahertz-frequency elastic waves, with two electronic ports on its upper facet, clear optical aperture D, and an effective acoustic absorber on its bottom facet [see Fig. 1(a)].

The first wave process represents mixing the longitudinal elastic waves of finite amplitudes in a compactly localized upper domain of a cell where a relatively powerful pump of the frequency f_p interacts with relatively weaker signal elastic wave of the frequency f_s. During just this nonlinear process, a collinear wave heterodyning takes place providing the appearance of an elastic wave of the difference frequency f_D, which is able to propagate along a large-aperture cell due to weaker manifestation of strongly dispersive losses at lower frequencies [see Fig. 1(b)].

The second wave process is the subsequent Bragg light scattering by the difference-frequency elastic wave in a pos-

0091-3286/2011/$25.00 © 2011 SPIE

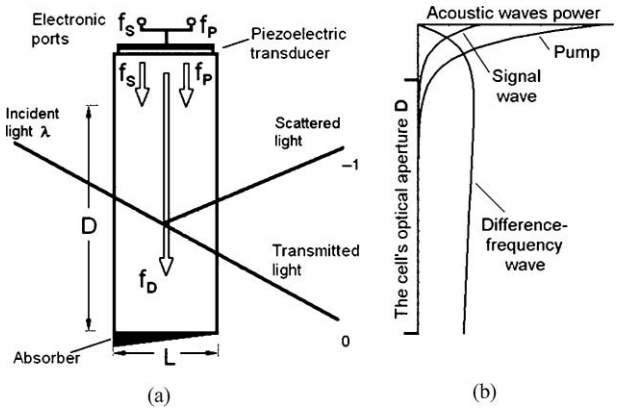

Fig. 1 Schematic arrangement of the interacting beams in (a) a two-cascade acousto-optical cell, and (b) the illustrating spatial distributions for powers of the interacting acoustic waves.

sible linear regime (i.e., in the regime of a given acoustic field for the incident light beam). This process occurs within a clear aperture D lighted by a wide incident optical beam of the wavelength λ (in air) and is able to realize optical spectrum analysis by itself. When, for example, the signal wave is rather intricate in behavior and consists of various frequencies, each individual spectral component from the difference-frequency elastic wave plays the role of a partial thick dynamic diffractive grating for the incident light beam. The length L of acousto-optical interaction has to provide performing the Bragg regime of light scattering.

Generally, the term "resolution" can be interpreted in slightly different ways from one another. One of these ways can be naturally related to the number N of resolvable spots, because increasing N undoubtedly means improving the resolution. Nevertheless, the resolution can be characterized from the other side as well if one will consider the absolute value of, for example, frequency resolution: because as less is an individual resolvable frequency interval as more is the frequency resolution. Moreover, within designing a system (for instance, for the star radio astronomy) one can meet a specific situation when it is so desirable to improve just an absolute value of the frequency resolution that the penalty for that, even in the form of decreasing N when the bandwidth of processing is not fixed, becomes acceptable. In connection with this refining, only the last option is the case under consideration here. Namely, we aspire first of all to improving the frequency resolution, while a reasonably large number N serves us to be an illustration that it could be done algorithmically in a multichannel parallel regime. Therefore, potentials peculiar to the acousto-optical spectrum analysis of a gigahertz frequency range radio-wave signals with essentially improved relative value of the frequency resolution, which can be on the order of 10^{-5} in our case, is considered by exploiting a new type of the acousto-optical cell made of a really effective KRS–5 cubic single crystal. The obtained estimations show that the elaborated approach, based algorithmically on a two-cascade processing, allows the direct 5000-channel parallel optical analysis of spectra inherent in ultrahigh-frequency radio-wave signals. In frames of the performed investigations, the efficiencies of both non-collinear acousto-optical and collinear acoustic interactions are analytically estimated. Moreover, analytic expression for the corresponding effective acoustic modulus of the third order in KRS–5 has been found for the first time in our knowledge. In so doing, contrary to our recently developed theoretical approach based on the technique of substantial approximations,[4,5] a regime of the coupled acoustic modes is considered, which provides more accurate analysis. These findings make it possible, first to estimate the technical requirements to performance data of the acousto-optical cell, as well as to acceptable values of the operating frequencies. At the end, previously proposed methodology for the experimental simulation[4] is practically applied and exploited within a specific example of the liquid-made cell to estimate performances of the parallel spectrum analysis with the new KRS–5-crystal–based acousto-optical cell.

2 Efficiency of Acousto-Optic Interaction in a KRS–5 Cubic Single Crystal

One can start from estimating the potential efficiency I of Bragg light scattering by the longitudinal acoustic waves in a KRS–5 single crystal. At first, let us take the cell's orientation shown in Fig. 2. Such a selection has its origins in preliminary known data related to linear and nonlinear manifestations of optical and acoustical properties inherent in this crystal.

To obtain the figure of acousto-optical merit M_2 inherent in the selected cut of a KRS–5 crystal, first of all the effective photoelastic constant p_{eff} must be found. For this purpose, one has to take into account that a KRS–5 single crystal belongs to the m3m cubic symmetry group. This crystal allows existing pure longitudinal elastic waves with the wave vector $\boldsymbol{K}$ and the displacement vector $\boldsymbol{u} = u\boldsymbol{m}$, when these waves are passing along the crystallographic axis [111], so that $\boldsymbol{K} \| \boldsymbol{m} \| [111]$. Each dynamic acoustic grating can be characterized by its deformation tensor of the second rank. Because of $\boldsymbol{K} \| [111]$ and $\boldsymbol{u} \| [111]$, one can write $\boldsymbol{q} = \boldsymbol{K}/|\boldsymbol{K}| = (1/\sqrt{3})(1, 1, 1)$ and $\boldsymbol{u} = (1/\sqrt{3})(1, 1, 1)$, so that the corresponding deformation tensor $\gamma^{(\mathrm{L})}$ takes the form

$$\gamma^{(\mathrm{L})} = \frac{1}{2}\,(\boldsymbol{u} \cdot \boldsymbol{q} + \boldsymbol{q} \cdot \boldsymbol{u}) = \frac{1}{3}\begin{pmatrix} 1 & 1 & 1 \\ 1 & 1 & 1 \\ 1 & 1 & 1 \end{pmatrix}. \tag{1}$$

The tensor $\gamma^{(\mathrm{L})}$ of the second rank with the components $\gamma_{kl}^{(L)}(k, l = 1, 2, 3)$ can be converted into a six-dimension vector $\tilde{\boldsymbol{\gamma}}^{(L)} = (1/3)(1, 1, 1, 2, 2, 2)$.[7] This expression for the deformation tensor makes it possible to estimate the velocity of the longitudinal wave. For this purpose, one can use the tensor C of elastic moduli of the second order. If now one will use the same procedure[7] and take the tensor C of the fourth rank for the KRS–5 crystal in the form of a 6×6

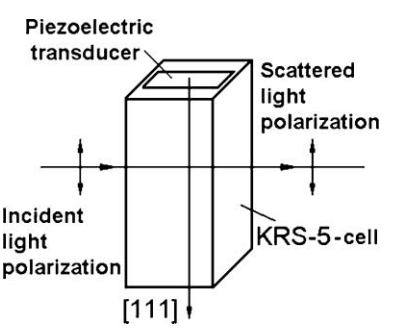

Fig. 2 Crystallographic orientations for the piezoelectric transducer and the crystalline material in a KRS–5 cell.

matrix, its components $C_{\lambda\mu}$ will be nonzero only with $C_{11} = C_{22} = C_{33}$, $C_{44} = C_{55} = C_{66}$, and $C_{12} = C_{13} = C_{21}$ $C_{23} = C_{31} = C_{32}$. Utilizing a similar representation, one can find the corresponding effective elastic modulus of the second order,

$$C_2 = \gamma^{(\mathrm{L})} C \gamma^{(\mathrm{L})} = \bar{\gamma}_{\lambda}^{(\mathrm{L})} C_{\lambda\mu} \bar{\gamma}_{\mu}^{(\mathrm{L})} = (1/3)\,(C_{11} + 2C_{12} + 4C_{44}), \quad (2)$$

which describes the velocity V_{L} inherent in the selected pure elastic longitudinal mode as $V_L = \sqrt{C_2/\rho}$, where ρ is the material density. One can use $C_{11} = 3.4 \times 10^{11}$ dyne/cm^2, $C_{12} = 1.3 \times 10^{11}$ dyne/cm^2, $C_{44} = 0.58 \times 10^{11}$ dyne/cm^2, and $\rho = 7.37$ g/cm^3 peculiar to a KRS–5 crystal and estimate $V_{\mathrm{L}} = 1.92 \times 10^5$ cm/s. Together with this, one must note that acoustic attenuation peculiar to this acoustic mode is not too low and is characterized by the factor $\Gamma = 10$ dB/(cm GHz^2).[8,9]

Now, one is ready to estimate the efficiency of acousto-optical interaction associated with the above-selected longitudinal elastic wave. By this we mean that the photoelastic tensor p of the fourth rank should be taken and converted into the form of a 6×6 matrix with the components $p_{\lambda\mu}$. For the cubic KRS–5 crystal (symmetry group m3m), matrix representation for the tensor p gives the following nonzero components: $p_{11} = p_{22} = p_{33}$, $p_{44} = p_{55} = p_{66}$, and $p_{12} = p_{13} = p_{21} = p_{23} = p_{31} = p_{32}$. Consequently, one can calculate the matrix product $p\bar{\gamma}^{(L)} = (1/3)(p_{11} + 2p_{12}, p_{11} + 2p_{12}, p_{11} + 2p_{12}, 2p_{44}, 2p_{44}, 2p_{44})$ and convert it back to the form of a standard tensor $[p\gamma^{(\mathrm{L})}]$ of the second rank.[7] The effective photoelastic constant can be written from the scalar form

$$p_{\mathrm{eff}} = \boldsymbol{e}_1 (p\gamma^{(\mathrm{L})}) \boldsymbol{e}_0 = \frac{1}{3}\,\boldsymbol{e}_1 \begin{pmatrix} p_{11}+2p_{12} & 2p_{44} & 2p_{44} \\ 2p_{44} & p_{11}+2p_{12} & 2p_{44} \\ 2p_{44} & 2p_{44} & p_{11}+2p_{12} \end{pmatrix} \boldsymbol{e}_0, \quad (3)$$

whereas before the vectors $\boldsymbol{e}_0$ and $\boldsymbol{e}_1$ describe the polarization states of incident and scattered light beams, respectively. Because of $\boldsymbol{K} \| [111]$, it is obvious that if the Bragg angles are omitted as small values, the wave vectors $\boldsymbol{k}_0$ and $\boldsymbol{k}_1$ of the incident and scattered light beams, respectively, should lie in the (111)-plane to be orthogonal to $\boldsymbol{K}$. Moreover, one can put $\boldsymbol{k}_0 = \boldsymbol{k}_1 = \boldsymbol{k}$ when the Bragg angles are neglected. Due to optical isotropy of cubic KRS–5 crystal, one can select, for example, $\boldsymbol{k} \| [1\bar{1}0]$. In this particular case, one has an opportunity to consider the vectors $\boldsymbol{e}_0$ and $\boldsymbol{e}_1$ belonging to $(1\bar{1}0)$-plane, which includes [110], [111], and [001] axes; therewith the axes [110] and [001] give us an orthogonal basis, because [110] $\perp$ [001]. In so doing, let us take at first the angles $\alpha_{0,1}$ as current angles between $\boldsymbol{e}_{0,1}$ and the [001]-axis. Consequently, one can easily obtain that $\boldsymbol{e}_{0,1} = (\sin\alpha_{0,1}/\sqrt{2}, \sin\alpha_{0,1}/\sqrt{2}, \cos\ \alpha_{0,1})$, so that $\boldsymbol{e}_{0,1} \| [001]$ when $\alpha_{0,1} = 0$. Now, one can change the initial position for the vectors $\boldsymbol{e}_{0,1}$ via the substitution the angles $\alpha_{0,1}$ by the new angles $\alpha_{0,1} + \beta_1$, where $\beta_1 = \arccos(1/\sqrt{3})$; i.e., one can write

$$\boldsymbol{e}_{0,1} = \left[\frac{1}{\sqrt{2}} \sin(\alpha_{0,1} + \beta_1),\ \frac{1}{\sqrt{2}} \sin(\alpha_{0,1} + \beta_1),\ \cos\,(\alpha_{0,1} + \beta_1) \right]. \quad (4)$$

After such a substitution, one will have finally obtained that $\boldsymbol{e}_{0,1} \| [111]$ when $\alpha_{0,1} = 0$. Usually, two types of light scattering can be realized. At first, one can consider the normal scattering when $\alpha_1 = \alpha_0$. In this case,

$$p_{\mathrm{eff}}^{(n)} = \frac{1}{3} \left\{ (p_{11} + 2p_{12} + 2p_{44})\ \sin^2(\alpha_0 + \beta_1) + 2\sqrt{2} p_{44} \times \sin[2(\alpha_0 + \beta_1)] + (p_{11} + 2p_{12})\ \cos^2(\alpha_0 + \beta_1) \right\}. \quad (5)$$

This formula can be simulated numerically with $p_{11} = 0.21$, $p_{12} = 0.22$, and $p_{44} = 0.15$ [see Fig. 3(a)]. The oscillating plot exhibits a maximum magnitude $p_{\mathrm{eff\,max}}^{(n)} = 0.417$ at $\alpha_0 = \pi k$, $k = \{\ldots, -2, -1, 0, 1, 2, \ldots\}$ and a minimum magnitude $p_{\mathrm{eff\,min}}^{(n)} = 0.117$ at $\alpha_0 = (\pi/2) + \pi k$. The second type is associated with the anomalous light scattering when $\alpha_1 = \alpha_0 + (\pi/2)$. Similar process is characterized by

$$p_{\mathrm{eff}}^{(an)} = \frac{p_{44}}{3} \left\{ \sin[2(\alpha_0 + \beta_1)] + 2\sqrt{2}\ \cos[2(\alpha_0 + \beta_1)] \right\}. \quad (6)$$

This value reaches provides its maxima $p_{\mathrm{eff\,max}}^{(an)} = 0.15$ with $\alpha_0 = (\pi/4) + (\pi k/2)$. The plots associated with these angular distributions for the effective photo-elastic constants in a KRS–5 single crystal are shown in Fig. 3(b). The maximal magnitude inherent in the corresponding figures of acousto-optical merit is related to the normal scattering in a KRS–5 single crystal and equal to $M_2 = n^6 (p_{\mathrm{eff\,max}}^{(n)})^2/(\rho V_{\mathrm{L}}^3) \approx 930 \times 10^{-18}$ s^3/g with $n = 2.57$ at the wavelength $\lambda = 671$ nm. The performed calculations demonstrate that the normal

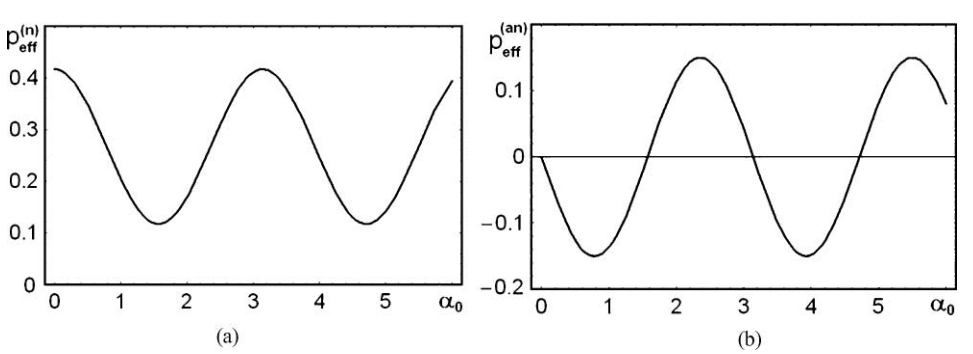

Fig. 3 Absolute dependences for the effective photoelastic constants in a KRS–5 single crystal versus the angle α_0: (a) normal light scattering and (b) anomalous light scattering.

light scattering by the longitudinal elastic wave is a few times more efficient than the anomalous one.

The other side of estimating the efficiency of acousto-optic interaction is connected with choosing the regime of light scattering. The most efficient one is the Bragg regime, which is shown in Fig. 1(a). It allows 100% efficiency of light scattering and occurs with large enough length L of interaction between light and acoustic waves when the dynamic acoustic diffractive grating is sufficiently thick. Such a regime can be realized only when the angle of light incidence on that acoustic grating meets the corresponding Bragg condition (which can be assumed to be provided in advance) and the inequality $Q = 2\pi\lambda L f_D^2/(nV_L^2) \gg 1$ for the Klein-Cook factor Q (Ref. 10) is satisfied. Taking, for example, $\lambda = 671$ nm, $L = 1.0$ cm, and $V_L = 1.92 \times 10^5$ cm/s, one can estimate $Q \geq 7$ for $f_D > 40$ MHz. Thus, the Bragg regime of light scattering could be expected for the acoustic difference frequencies at least exceeding 40 MHz in a KRS–5 single crystal, so that the acoustic frequency $f_D = 40$ MHz can be considered as a lower limit for the Bragg regime of light scattering.

3 Efficiency of the Codirectional Collinear Acoustic Wave Heterodyning

At this stage, effect of a three-acoustic wave mixing associated with the longitudinal elastic wave propagating along the [111]-axis in a KRS–5 single crystal is under consideration. It can be done using the Shapiro–Thurston equation[11] reduced down to terms of the third order in its general form,

$$\rho\frac{\partial^2 u_i}{\partial t^2} - C_{ijkl}\frac{\partial^2 u_k}{\partial x_j \partial x_l} = \tilde{C}_{ijklqr}\frac{\partial u_q}{\partial x_r}\frac{\partial^2 u_k}{\partial x_j \partial x_l}, \tag{7}$$

$$\tilde{C}_{ijklqr} = C_{ijklqr} + C_{ijlq}\delta_{kr} + C_{ilqr}\delta_{jk} + C_{iklq}\delta_{jr}. \tag{8}$$

These equations include all the components. In the above-chosen case of propagating pure longitudinal elastic mode along the crystallographic axis [111] with $\boldsymbol{K}\|\boldsymbol{m}\|[111]$ (see Sec. 2), the direction cosines $n_i (i = 1,2,3)$ should satisfy a pair of the following obvious conditions $n_1 = n_2 = n_3$ and $n_1^2 + n_2^2 + n_3^2 = 1$, so that $n_i = 1/\sqrt{3}$. Using Eqs. (7) and (8), and after easy but cumbersome algebraic calculations, one can obtain the following effective elastic modulus of the third order:

$$\begin{aligned} C_3 = {} & C_{111} + 2C_{123} + 6C_{112} + 12C_{144} + 16C_{456} \\ & + 24C_{155} + 9C_{11} + 18C_{12} + 36C_{44} \end{aligned} \tag{9}$$

and (exploiting, for example, the data from Ref. 12) conclude that the longitudinal elastic wave propagating along the [111]-axis is definitely capable of mixing the acoustic waves in a KRS–5 single crystal.

Now, one can introduce the new coordinate axis x oriented along the [111] crystallographic axis of KRS–5, so that $\boldsymbol{x}\|\boldsymbol{m}\|[111]$ and Eq. (7) takes the form

$$\frac{\partial^2 u}{\partial t^2} - V_L^2\frac{\partial^2 u}{\partial x^2} = \frac{C_3}{\rho}\frac{\partial u}{\partial x}\frac{\partial^2 u}{\partial x^2}. \tag{10}$$

The first term in Eq. (10) can be approximately converted within the quasi-linear linear form of $\partial u/\partial x \approx -V_L(\partial u/\partial x)$ as $\partial^2 u/\partial t^2 \approx -V_L(\partial^2 u/\partial x \partial t)$. Then, using the obvious relation $2(\partial u/\partial x)(\partial^2 u/\partial x^2) = (\partial/\partial x)(\partial u/\partial x)^2$, one can integrate Eq. (10) with respect to x. After that, an additional phenomenological term $\alpha V_L u$ can be included to take into account linear acoustic losses, which are physically characterized by the amplitude decrement α (measured in centimeters to the power –1), reflecting usually just the square-law frequency dispersion of losses in solids. As a result, one can write

$$\frac{\partial u}{\partial t} + V_L\frac{\partial u}{\partial x} + \alpha V_L\, u = \frac{\Gamma}{2}V_L\left(\frac{\partial u}{\partial x}\right)^2, \tag{11}$$

where $\Gamma = -C_3/C_2$, $V_L = \sqrt{C_2/\rho}$, and $C_2 = (C_{11} + C_{12} + C_{44})/3$ is the elastic modulus of the second order for $\boldsymbol{x}\|\boldsymbol{m}\|[111]$. A one-dimensional wave equation [Eq. (11)] for the complex amplitude of an elastic wave is peculiar for characterizing a three-wave mixing in a medium with linear dispersive losses and square-law nonlinearity. Because of a square-law dispersion of acoustic losses, the complex amplitude u can be taken in the form of a superposition of only a triplet of waves, including the pump, the signal wave, and the difference-frequency wave, namely, $u = u_P + u_S + u_D$, while the second harmonics of both the pump and the signal wave as well as their sum-frequency component can be omitted in this project of the chosen solution. Starting, for example, from the pump, one can write the corresponding complex amplitude as $u_P(x,t) = A_P(x)\exp[i(k_P x - \omega_P t)] + A_P^*(x)\exp[-i(k_P x - \omega_P t)]$ and note its losses as α_P. Substituting this formula into the left-hand side of Eq. (11), one can calculate

$$\begin{aligned} & V_L^{-1}\frac{\partial u_P}{\partial t} + \frac{\partial u_P}{\partial x} + \alpha_P u \\ & \quad = \left[\alpha_P A_P + \frac{dA_P}{dx}\right]\exp[i(k_P x - \omega_P t)] \\ & \qquad + \left[\alpha_P A_P^* + \frac{dA_P^*}{dx}\right]\exp[-i(k_P x - \omega_P t)]. \end{aligned} \tag{12}$$

It is seen that the relations analogous to Eq. (12) can be obtained for the signal and difference-frequency waves. To construct the contribution $(\partial u/\partial x)^2$ in the right-hand side of Eq. (11) one has to estimate the summands. Applying the slowly varying amplitudes technique, one must take into account the inequalities $|dA_j(x)/dx| \ll k_j|A_j(x)|$, $j \in [P,S,D]$. Consequently, the following approximation appears

$$\begin{aligned} \left(\frac{\partial u}{\partial x}\right)^2 \approx {} & \big(ik_P\{A_P(x)\exp[i(k_P x - \omega_P t)] \\ & - A_P^*(x)\ \exp[-i(k_P x - \omega_P t)]\} \\ & + ik_S\{A_S(x)\ \exp[i(k_S x - \omega_S t)] \\ & - A_S^*(x)\ \exp[-i(k_S x - \omega_S t)]\} \\ & + ik_D\{A_D(x)\ \exp[i(k_D x - \omega_D t)] \\ & - A_D^*(x)\ \exp[-i(k_D x - \omega_D t)]\}\big)^2. \end{aligned} \tag{13}$$

Now, one must consider two different regimes of a three-wave mixing. The right-hand sides of Eqs. (12) and (13) give

1. $f_S = f_P + f_D$:

$$\frac{dA_S}{dx} + \alpha_S A_S = \beta_S A_D A_P, \tag{14a}$$

$$\frac{dA_P}{dx} + \alpha_P A_P = -\beta_P A_D^* A_S, \tag{14b}$$

$$\frac{dA_D}{dx} + \alpha_D A_D = -\beta_D A_P^* A_S; \tag{14c}$$

2. $f_P = f_S + f_D$:

$$\frac{dA_P}{dx} + \alpha_P A_P = \beta_P A_D A_S, \tag{15a}$$

$$\frac{dA_S}{dx} + \alpha_S A_S = -\beta_S A_D^* A_P, \tag{15b}$$

$$\frac{dA_D}{dx} + \alpha_D A_D = -\beta_D A_S^* A_P. \tag{15c}$$

where $\beta_S = 0.5\,\Gamma\, k_P k_D$, $\beta_P = 0.5\,\Gamma\, k_S k_D$, and $\beta_D = 0.5\,\Gamma\, k_P k_S$ are the coupling factors. At this step, one can take $A_{D,S,P} = a_{D,S,P}\,\exp\,[i(\varphi_{D,S,P})]$, where $a_{D,S,P}$ and $\varphi_{D,S,P}$ are the real-valued amplitudes and phases of non-optical waves. Let us consider, for example, Eq. (14) governing the system in a regime of $f_S = f_P + f_D$ with $\mathrm{sign}(f_P - f_S) = -1$. Dividing real and imaginary parts in Eq. (14), one can find two groups of the real-valued equations

$$\frac{da_S}{dx} + \alpha_S a_S = \beta_S a_D a_P\,\cos\,(\varphi_S - \varphi_D - \varphi_P), \tag{16a}$$

$$\frac{da_D}{dx} + \alpha_D a_D = -\beta_D a_S a_P\,\cos\,(\varphi_S - \varphi_D - \varphi_P), \tag{16b}$$

$$\frac{da_P}{dx} + \alpha_P a_P = -\beta_P a_D a_S\,\cos\,(\varphi_S - \varphi_D - \varphi_P); \tag{16c}$$

$$\frac{d\varphi_S}{dx} a_S = \beta_S a_D a_P\,\sin\,(\varphi_S - \varphi_D - \varphi_P), \tag{17a}$$

$$\frac{d\varphi_D}{dx} a_D = -\beta_D a_S a_P\,\sin\,(\varphi_S - \varphi_D - \varphi_P), \tag{17b}$$

$$\frac{d\varphi_P}{dx} a_P = -\beta_P a_D a_S\,\sin\,(\varphi_S - \varphi_D - \varphi_P). \tag{17c}$$

Equations (16) and (17) can be analyzed with the natural for similar problems boundary conditions $U_P \neq 0$, $U_S \neq 0$, and $U_D = 0$, where $U_{P,S,D} = A_{P,S,D}(x = 0)$. With these conditions, one can find from Eq. (16b) that $(da_D/dx)(x = 0) = -\beta_D U_P U_S$. Here, the following quite natural approximation can be done; namely, let us put $a_P \gg a_S$, a_D almost everywhere in an area of interaction. In this particular case, Eq. (16c) can be solved in a given field approximation as $a_P = U_P\,\exp(-\alpha_P x)$, while Eq. (17c) gives $d\varphi_P/dx = 0$. Substituting these solutions into Eqs. (16) and (17) and dividing real and imaginary parts, one can obtain

$$\frac{da_S}{dx} + \alpha_S a_S = \beta_S a_D U_P\,\exp\,(-\alpha_P x)\,\cos\,\varphi, \tag{18a}$$

$$\frac{da_D}{dx} + \alpha_D a_D = -\beta_D a_S U_P\,\exp\,(-\alpha_P x)\,\cos\,\varphi, \tag{18b}$$

$$\frac{d\varphi}{dx} = U_P\,\exp(-\alpha_P x)\,\sin\,\varphi\,\left(\beta_D\,\frac{a_S}{a_D} - \beta_S\,\frac{a_D}{a_S}\right), \tag{18c}$$

$$\varphi = \varphi_S - \varphi_P - \varphi_D. \tag{18d}$$

From the first integral of Eq. (18), with allowance for the boundary condition $a_D(x = 0) = 0$, which is characteristic of wave heterodyning, one can find that $\mathrm{d}\varphi/\mathrm{d}x \equiv 0$ and $\sin\,\varphi \equiv 0$, so that one can take, for example, $\cos\varphi = 1$. Equations (15a)–(15c), associated with the regime $f_P = f_S + f_D$ with $\mathrm{sign}\,(f_P - f_S) = +1$, can be analyzed by similar way via substituting $\beta_S \to -\beta_S$. Consequently, Eqs. (18a) and (18b) give the two following pairs of the combined ordinary differential equations of the first order:

$$\frac{da_S}{dx} + \alpha_S a_S = -\,\mathrm{sign}\,(f_P - f_S)\,\beta_S a_D U_P\,\exp\,(-\alpha_P x), \tag{19a}$$

$$\frac{da_D}{dx} + \alpha_D a_D = -\beta_D a_S U_P\,\exp\,(-\alpha_P x). \tag{19b}$$

Excluding a_S from Eq. (19), one can write a linearized version for the needed second-order ordinary differential equation

$$\frac{d^2 a_D}{dx^2} + (\alpha_P + \alpha_S + \alpha_D)\frac{da_D}{dx} + \big[\alpha_D(\alpha_P + \alpha_S) - \mathrm{sign}\,(f_P - f_S)\,\beta_S\beta_D U_P^2 \exp\,(-2\alpha_P x)\big]a_D = 0. \tag{20}$$

Because of the above-mentioned dispersion of losses included in the factors α_P, α_S, and α_D, one can extract their square-law proportionalities to the corresponding carrier frequencies of acoustic waves $\alpha_{P,S,D} \sim f_{P,S,D}^2$ and write

$$\alpha_P + \alpha_S + \alpha_D = 2\alpha_P[1 + \delta\,\mathrm{sign}\,(f_P - f_S) + \delta^2], \tag{21a}$$

$$\alpha_P + \alpha_S - \alpha_D = 2\alpha_P\,[1 + \delta\,\mathrm{sign}\,(f_P - f_S)], \tag{21b}$$

with $\delta = f_D/f_P \ll 1$. Introducing the notations $g = -\,\delta\,\mathrm{sign}\,(f_P - f_S) + \delta^2$ and $h = \delta\,\mathrm{sign}(f_P - f_S)$ so that $g \approx -\,h$ due to the smallness of δ, one can express the exact solution to Eq. (20) in terms of the Bessel functions as

$$a_D(x) = \exp\,[-\alpha_P x(1 + g)]\,\{C_1 Z_{(h-1)}\,[\xi\,\exp\,(-\alpha_P x)] + C_2 Z_{(1-h)}\,[\xi\,\exp\,(-\alpha_P x)]\}, \tag{22}$$

where $\xi = \alpha_P^{-1} U_P \sqrt{\beta_S \beta_D}$ is the normalized acoustic wave amplitude. Then, $Z_\nu = J_\nu$ when $f_P < f_S$ and $\mathrm{sign}(f_P - f_S) = -1$, while $Z_\nu = I_\nu$ with $f_P > f_S$ and $\mathrm{sign}(f_P - f_S) = +1$ (for example, see Ref. 13). Exploiting the

above-mentioned boundary conditions for a_D and its spatial derivative, one can determine the constants $C_{1,2}$ of integration in Eq. (22) as

$$C_1 = \left(\frac{-2\beta_D U_P U_S}{\alpha_P \xi}\right) \frac{Z_{(1-h)}(\xi)}{W(\xi, h)}, \tag{23a}$$

$$C_2 = \left(\frac{2\beta_D U_P U_S}{\alpha_P \xi}\right) \frac{Z_{(h-1)}(\xi)}{W(\xi, h)}, \tag{23b}$$

$$W(\xi, h) = Z_{(1-h)}(\xi)[Z_{(h-2)}(\xi) + \text{sign}\,(f_P - f_S)\, Z_{(h)}(\xi)] - Z_{(h-1)}(\xi)[Z_{(-h)}(\xi) + \text{sign}\,(f_P - f_S)\, Z_{(2-h)}(\xi)]. \tag{24}$$

Thus, Eqs. (22)–(24) represent the solution describing the spatial distribution for the difference-frequency acoustic wave along the acousto-optical cell exploiting collinear acoustic wave heterodyning. In the above-noted particular cases, Eq. (24) can be simplified as $W(\xi, h) = -4(\pi\ \xi)^{-1}\ \sin(\pi\ \delta)\ \text{sign}\,(f_P - f_S)$, so that one can write

1. $f_S = f_P + f_D$, $\text{sign}\,(f_P - f_S) = -1$:

$$a_D(\alpha_P x) = \frac{\pi\beta_D U_P U_S\{J_{(-\delta-1)}(\xi)J_{(1+\delta)}[\xi\ \exp(-\alpha_P x)] - J_{(1+\delta)}(\xi)J_{(-\delta-1)}[\xi\ \exp(-\alpha_P x)]\}}{2\alpha_P \sin(\pi\delta)\ \exp[\alpha_P x(1+\delta+\delta^2)]}, \tag{25}$$

2. $f_P = f_S + f_D$, $\text{sign}\,(f_P - f_S) = +1$:

$$a_D(\alpha_P x) = \frac{\pi\beta_D U_P U_S\{I_{(1-\delta)}(\xi)I_{(\delta-1)}[\xi\ \exp(-\alpha_P x)] - I_{(\delta-1)}(\xi)I_{(1-\delta)}[\xi\ \exp(-\alpha_P x)]\}}{2\alpha_P \sin(\pi\delta)\ \exp[\alpha_P x(1-\delta+\delta^2)]}. \tag{26}$$

The amplitude distributions, which are inherent in the difference-frequency acoustic wave components and normalized by the factor $\pi\beta_D U_P U_S/(2\alpha_P)$, for the same pairs of the normalized acoustic wave amplitudes ξ are presented in Figs. 4 and 5.

4 Estimating the Frequency Potentials Peculiar to Multichannel Direct Optical Spectrum Analysis with Novel Acousto-Optical Cell

Potential Estimating frequency limitations can be analyzed within nonlinear acoustic mechanisms of collinear heterodyning. Without the loss of generality, let us take Eq. (25) for further analysis at length. This equation, related as before to the case of $f_S = f_P + f_D$, can be rewritten with $z = \alpha_P x$ as

$$a_D(z) = F_D\ \Phi\ (z, \delta, \xi), \tag{27a}$$

$$F_D = \frac{\pi\beta_D U_P U_S}{2\alpha_P}, \tag{27b}$$

$$\Phi\ (z, \delta, \xi) = \frac{J_{(-\delta-1)}(\xi)J_{(1+\delta)}[\xi\ \exp(-z)] - J_{(1+\delta)}(\xi)J_{(-\delta-1)}[\xi\ \exp(-z)]}{\sin(\pi\delta)\ \exp[z(1+\delta+\delta^2)]}. \tag{27c}$$

At this stage, the coordinate z_m of a maximum of the amplitude function $\Phi(z,\delta,\xi)$ must be found. For this purpose, one must analyze the condition $[d\Phi\ (z_m, \delta, \xi)/dz] = 0$. The condition of an existing maximum for $\Phi(z,\delta,\xi)$ takes the form

$$J_{(-1-\delta)}(\xi)\{\delta^2 J_{(1+\delta)}[\xi\exp(z_m)] + \xi\exp(z_m)J_{(\delta)}[\xi\exp(z_m)]\} - J_{(1+\delta)}(\xi)\{\delta^2 J_{(-1-\delta)}[\xi\exp(z_m)] - \xi \times \exp(z_m)J_{(-\delta)}[\xi\exp(z_m)]\} = 0. \tag{28}$$

This condition can be easily analyzed numerically by considering δ and z_m as the independent and dependent variables, respectively, while ξ plays the role a discrete independent parameter. One can find from Eq. (28) that

$$z_m(\delta, \xi = 0.5) \approx 2.66 - 2.1\times10^{-4}\,\delta^{-2} + 0.0405\,\delta^{-1} - 8.17\,\delta + 10.3\,\delta^2, \tag{29a}$$

$$z_m(\delta, \xi = 1.0) \approx 2.587 - 6.0\times10^{-6}\,\delta^{-2} + 0.0016\,\delta^{-1} - 8.26\,\delta + 11.4\,\delta^2; \tag{29b}$$

see Fig. 6(a). These formulas are rather important practically because they make it possible to estimate potential frequency limitations for optical spectrum analysis.

On one side, substituting the obtained $z_m(\delta,\xi)$ into Eq. (28) allows us, first, to estimate the accuracy of the performed approximations. Figure 6(b) illustrates the closeness of the

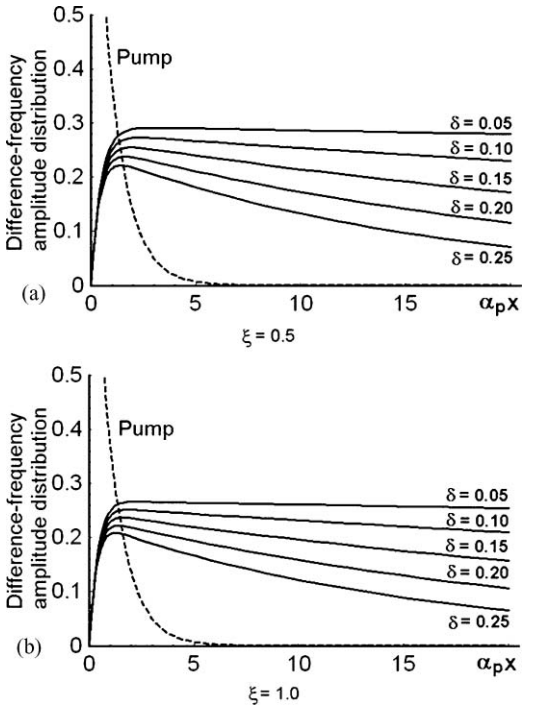

Fig. 4 Normalized amplitudes for the difference-frequency acoustic waves versus the product $\alpha_P x$ when $f_S = f_P + f_D$.

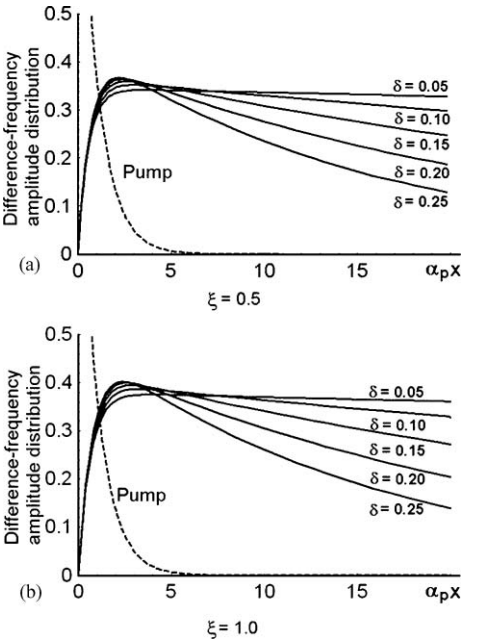

Fig. 5 Normalized amplitudes for the difference-frequency acoustic waves versus the product $\alpha_P x$ when $f_P = f_S + f_D$.

derivative $d\Phi\,[z_m(\boldsymbol{\delta}, \boldsymbol{\xi}), \boldsymbol{\delta}, \boldsymbol{\xi}]/dz$ to zero in terms of its relative fall off from zero for two particular cases of $\xi = 0.5$ and $\xi = 1.0$. One can see from Fig. 6(b) that the maximal value of an error does not exceed 0.3% within $\delta \in [0.01;0.30]$. Then, Figs. 4 and 5 exhibit a nonuniformity of distributing signals associated with various difference-frequency acoustic components inside the cell, so that a larger non-uniformity is associated with the component of a higher value of δ. Thus, one can take the upper difference-frequency component and restrict itself by an upper value δ_U of the parameter $\boldsymbol{\delta}$. Then, substituting the obtained $z_m(\delta_U,\xi)$ into $\Phi(z,\delta,\xi)$ makes it possible to formulate the requirement to the cell's optical aperture. One can see it as follows: decreasing the normalized acoustic field distribution down to a level of –3 dB along the cell's optical aperture at a point $z_D(\delta_U,\xi)$ gives the equality

$$\Phi^2[z_D(\delta_U, \xi), \delta_U, \xi] = 0.5\ \Phi^2[z_m(\delta_U, \xi), \delta_U, \xi] \tag{30}$$

in terms of the intensities.

In fact, the value of $z_D(\delta_U,\xi)$ determines the total geometric length $x_D(\delta_U,\xi)$ of an acousto-optical cell with the collinear wave heterodyning. Then, one can explain $x_{m,D} = \alpha_P^{-1}\, z_{m,D}$ and obtain

$$D = x_D(\delta_U, \xi) - x_m(\delta_U, \xi), \tag{31}$$

where D is the really operating part of the cell's optical aperture available for parallel optical processing at given ξ and some range of the parameter δ. Nevertheless, it is seen from Figs. 4 and 5 that the normalized intensity distributions $\Phi^2\,(z, \delta, \xi)$ are the obviously decreasing functions of the parameter δ. As a result, similar dependences on δ lead to a nonuniformity of distributing signals associated with various difference-frequency components inside the cell. Moreover, this nonuniformity is as large as the corresponding parameter δ is high, so that the lowest magnitude δ_L of the parameter δ leads to almost uniform acoustic signal distribution along the cell's optical aperture. Together with this, Figs. 4 and 5 show that the parameter δ is as high, as the absolute maximum of the corresponding dependence is low, and consequently,

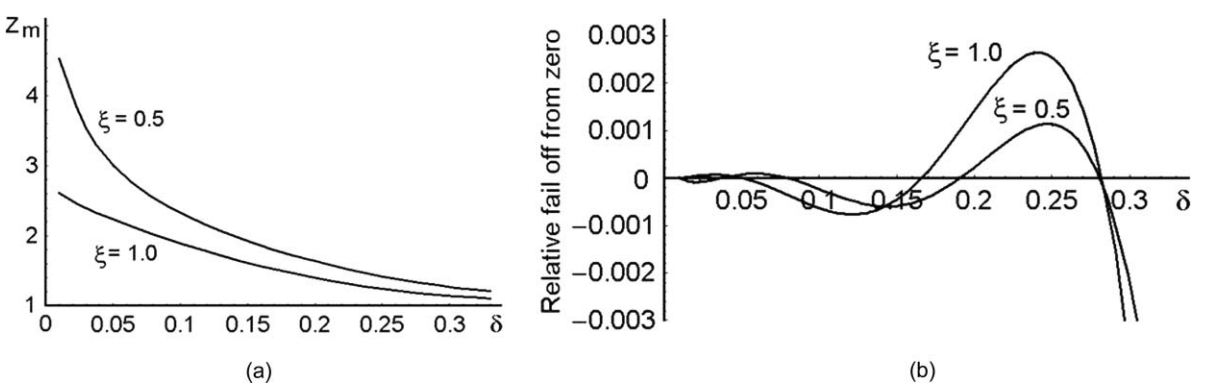

Fig. 6 (a) Plots determine the coordinate z_m as an approximate function of the frequency ratio δ from numerical solution to Eq. (28), whereas (b) curves characterize the relative accuracy of approximate plots in Fig. 6(a).

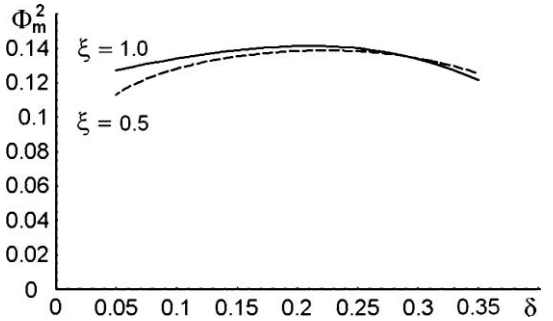

Fig. 7 Renormalized maximal intensities $\Phi_m^2\,[z_m(\delta), \delta, \xi]$ versus the parameter δ with $G = 4$: the dashed line is for $\xi = 0.5$, whereas the solid line is for $\xi = 1.0$.

the corresponding frequency components must be adequately preamplified. Under these circumstances, one can suggest the following criterion for such a preamplification, namely, let us equalize various frequency components in a central vicinity of the above-noted operating part D inherent in the cell's optical aperture. In so doing, one can suggest renormalizing maximal intensity determined by the expression

$$\Phi_m^2\,[z_m(\delta, \xi), \delta, \xi, G] = \frac{G}{z_m(\delta, \xi)}\,\Phi^2\,[z_m(\delta, \xi), \delta, \xi] \quad (32)$$

with possible linear gain G, whose magnitude can be taken rather arbitrarily. The corresponding distributions, both allowing δ_U up to 0.35 and δ_L down to 0.05, are presented in Fig. 7 in the particular case of, for instance, $G = 4$. This diagram illustrates the simplest (and definitely nonoptimized) possibility of the above-noted equalizing the frequency components involved.

Then, one can consider the renormalized spatial intensity distributions

$$\Phi_0^2\,(z, \delta, \xi) = \frac{G}{z_m(\delta)}\,\Phi^2\,(z, \delta, \xi) \quad (33)$$

along the cell's aperture. These distributions are depicted in Fig. 8 in the same particular case of $G = 4$ as before, together with the magnitudes $\delta_U = 0.17$ and $\delta_L = 0.034$, also taken, for example, in view of the further consideration.

Taking into account Eq. (30), one can find from Fig. 8 that the really operating part D of the cell's optical aperture available for parallel optical processing in Eq. (31) is practically independent on the magnitude of ξ. Very slight dependence on ξ manifests itself mainly in concrete localization of D within total aperture of the cell. However, this dependence is rather weak because it follows from the data in Fig. 8, so that potentially it could be neglected in practice.

At this point, an opportunity exists to simplify the process of determining the value of $x_D(\delta_U, \xi)$. In so doing, let us rewrite Eq. (27c) as $\Phi\ (z, \delta, \xi)\ = \Phi_1 + \Phi_2$, where

$$\Phi_1\,(z, \delta, \xi)\ = \frac{J_{(-\delta-1)}(\xi)J_{(1+\delta)}[\xi\ \exp\,(-z)]}{\sin\,(\pi\delta)\ \exp\,[z(1+\delta+\delta^2)]}, \quad (34a)$$

$$\Phi_2\,(z, \delta, \xi)\ = \frac{-J_{(1+\delta)}(\xi)J_{(-\delta-1)}[\xi\ \exp\,(-z)]}{\sin\,(\pi\delta)\ \exp\,[z(1+\delta+\delta^2)]}. \quad (34b)$$

Comparisons of these contributions to the right from the planes $z_m(\delta)$ in two above-chosen cases of $\xi = 0.5$ and $\xi = 1.0$ are presented in Fig. 9. It is clearly seen from Fig. 9 that $\Phi_1 \to 0$ and $\Phi_1 \ll \Phi_2$ in those areas, so that one can motivatively take the reduced form of $\Phi\ (z, \delta, \xi)$ and put $\Phi\ (z, \delta, \xi)\ \approx \Phi_2\ (z, \delta, \xi)$ within at least $z \geq 2z_m(\delta, \xi)$ in Eq. (27b) and take the reduced, but well-approximated form of Eq. (27a),

$$a_{DR}\,(z)\ = -\left(\frac{\pi\beta_D U_P U_S}{2\alpha_P}\right)\frac{J_{(1+\delta)}(\xi)J_{(-\delta-1)}\left[\xi\ \exp\,(-z)\right]}{\sin\,(\pi\delta)\ \exp\,[z(1+\delta+\delta^2)]}. \quad (35)$$

The corresponding contributions after substituting $\Phi\ (z, \delta, \xi)\ \approx \Phi_2\ (z, \delta, \xi)$ into Eq. (33) (i.e., after normalizing) are presented in Fig. 10 with $\delta = 0.17$ in the cases of $\xi = 0.5$ and $\xi = 1.0$ under discussion.

Now, let us direct our attention to the particular case of a KRS–5 crystalline cell with $\Gamma_0 = 10$ dB/(cm GHz^2) and practically operating optical aperture $D = 5.0$ cm and make a few practical estimations. At first, to provide higher operating frequencies inherent in the cell under consideration together with the simplicity of realizing a low-frequency pump, it looks preferable to choose an area of $f_S = f_P + f_D$ and sign $(f_P - f_S) = -1$ related to Eq. (25) in spite of the fact that this area is more sensitive to variations of the parameter δ (see Fig. 4). Applying Eq. (35) and Fig. 10, one can find that the upper difference frequency about $f_{UD} \approx 250$ MHz provides a ~3 dB level of acoustic losses along the taken optical aperture $D \approx 5.0$ cm of the cell. It should be noted at this step that the numerical estimations adduced here

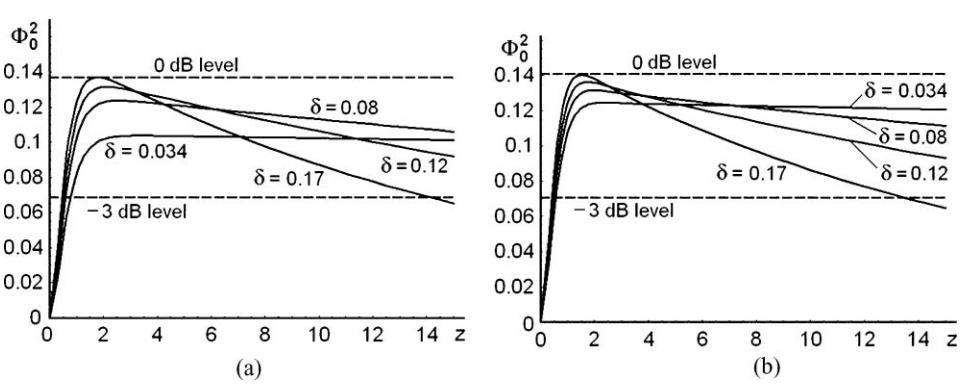

Fig. 8 Renormalized spatial intensity distributions $\Phi_0^2\,(z, \delta, \xi)$ along the cell's aperture with $G = 4$ for various δ: (a) is for $\xi = 0.5$ and (b) is for $\xi = 1.0$.

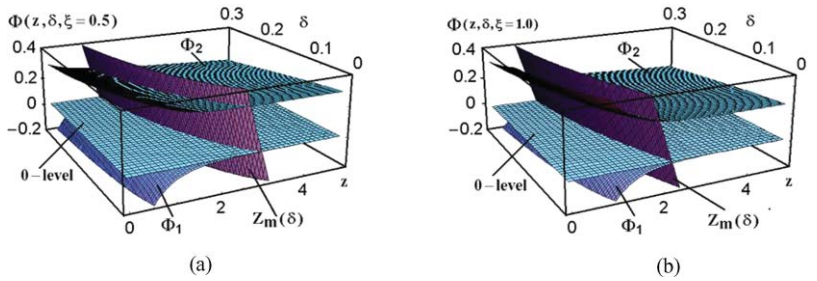

Fig. 9 Comparing the contributions of the terms Φ_1 and Φ_2 from Eq. (34) to the right of the plane $z_m(\delta,\xi)$ with (a) $\xi = 0.5$ and (b) $\xi = 1.0$. The 0 dB-levels are shown as well for a convenience.

should be considered as rather simplified illustrations, while practically notable technical calculations must be performed much more precisely. Nevertheless, one can say that these estimations reflect the proposed principle of operation in the full measure. Because of the upper magnitude of δ in this case is $\delta_U = 0.17$, as it follows also from Fig. 10, and initial determination of the parameter δ gives $f_{UD}/\delta_U = f_P$, one can find that the pump frequency will be $f_P = 1470$ MHz and the upper signal frequency will be $f_{US} = 1720$ MHz. Then, one can choose the bandwidth Δf of spectrum analysis, for example, in the range of 200 MHz, which leads to the lower difference frequency $f_{LD} = 50$ MHz restricted by the Bragg regime condition (see the corresponding estimation at the end of Sec. 2). Consequently, the lower signal frequency is $f_{LS} = 1520$ MHz, and the lower magnitude of the parameter δ is $\delta_L = 0.034$. These estimations are conditioned by the relations

$$f_{UD} = f_{US} - f_P = f_P\,\delta_U, \tag{36a}$$

$$f_{LD} = f_{LS} - f_P = f_P\,\delta_L. \tag{36b}$$

It should be noted that direct exploitation of similar KRS–5 cell with the active optical aperture $D = 5.0$ cm at the signal frequencies of already 1000 MHz is definitely impossible because the acoustic attenuation is ~50 dB along this aperture. Nevertheless, applying the collinear acoustic wave heterodyning allows us to operate on these gigahertz-range carrier frequencies. The above-mentioned nonuniformities in the distributions of signals associated with various difference-frequency components in the KRS–5 cell under consideration are illustrated in Fig. 8. Using Eq. (29) at the pump frequency $f_P = 1470$ MHz providing $\boldsymbol{\alpha}_P = 2.485$ cm^{-1}, one can estimate with $\delta_U = 0.17$ that $z_m = 1.80$ and $x_m = 0.720$ cm for $\xi = 0.5$ as well as $z_m = 1.52$ and $x_m = 0.608$ cm for $\xi = 1.0$. Then, estimating these non-uniformities in the distributions of acoustical signals along the cell's aperture at $\delta_U = 0.17$ even graphically makes it possible to conclude from Figs. 8 and 10 that one can obtain $z_D = 14.2$ and $x_D = 5.71$ cm for $\xi = 0.5$ as well as $z_D = 13.8$ and $x_D = 5.55$ cm for $\xi = 1.0$. At this point, it is worthwhile to make two refining remarks. First, the analysis should naturally include considering the behavior of another frequency component inherent in the complete spectrum of the difference-frequency signal, in particular, the component with $\delta_L = 0.034$. Nevertheless, one can see from Fig. 8 (as well as from Figs. 4 and 5) that total irregularity inherent in this lowest-frequency component is practically insignificant, even taking into account the appropriateness $z_m(\delta_L) > z_m(\delta_U)$. Second, some small part of the cell's aperture placed to the left of $\mathbf{z_m(\delta_U)}$, which exhibit more or less an "acceptable" level of signal irregularity can be also exploited practically. Thus, the real operating optical aperture D, lying between $z_m(\delta_U)$ and $z_D(\delta_U)$ for $\delta_U = 0.17$ at a level of –3 dB with the above-mentioned remarks, consists of approximately $D = 5.0$ cm.

5 Estimating the Efficiency of Collinear Wave Heterodyning

Now, the efficiency of collinear wave heterodyning in the chosen regime of a given pump intensity and coupling between signal and difference-frequency acoustic modes must be estimated. Again, without the loss of generality, let us take Eq. (25) in the form of Eq. (27), which describes the case of $f_S = f_P + f_D$, for further analysis. At this case, let us estimate the contributions involved in the term F_D from Eq. (27), which does not include any coordinate dependence contrary to the function $\Phi\ (z, \delta, \xi)$. One can start from the pump losses that are described by the factor $\boldsymbol{\alpha}_P = \tilde{\Gamma}_0\, f_P^2$.

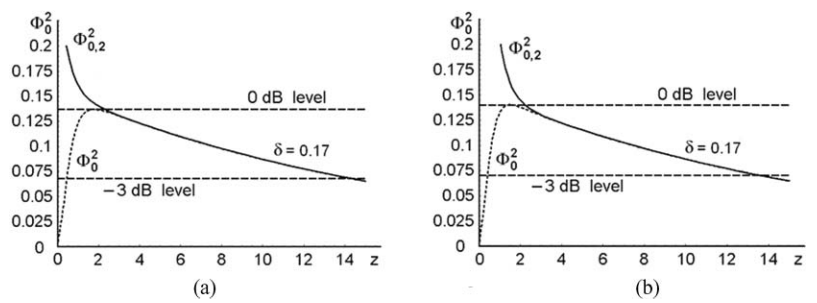

Fig. 10 Coinciding the terms Φ_0^2 and $\Phi_{0,2}^2$ obtained from Eqs. (33) and (34) to the right of the area $2z_m(\delta,\xi)$ with $G = 4$, $\delta = 0.17$ and (a) $\xi = 0.5$ and (b) $\xi = 1.0$. The 0 dB and –3 dB levels are shown as well.

Usually, the acoustic attenuation factor Γ_0 is used in bibliography (see, for instance, Refs. 8 and 9), measured in decibels per centimeter per gigahertz squared, but here one needs it in the form of $\tilde{\Gamma}_0$ (in seconds squared per centimeter) $= [(\ln 10)/10] \times 10^{-18} \cdot \Gamma_0$ dB/(cm GHz^2) within estimating the efficiency of collinear wave heterodyning. Then, the factor β_D, introduced in Eqs. (14) and (15), takes the form $\beta_D = 2\pi^2 V_L^{-2} \Gamma f_P f_S$. Finally, the deformation tensor $\gamma^{(L)}$, described initially by Eq. (1) in the normalized form, can be converted to the axes chosen in connection with orienting the coordinate axis x as $\boldsymbol{x}||\boldsymbol{m}||[111]$ in Eq. (10). In so doing, one can write $\gamma^{(L)} = \boldsymbol{u} \cdot \boldsymbol{q}$ for the longitudinal acoustic mode. After that, recovering the magnitudes of the vectors included into $\gamma^{(L)}$, one can explain the unique nonzero component of this tensor in dimensional form as $\gamma_j^{(11)} \equiv \gamma_j = U_j k_j$, where $j \in$ [P,S,D] as before [see comments to Eq. (13)]. This dimensional form represents a scalar relation as well, so that it can be inverted as $U_j = \gamma_j / k_j$, where $k_j = 2\pi f_j / V_L$. In its turn, the chosen component of deformations can be explained in terms of the corresponding acoustic power density P_j as $\gamma_j^2 = 2P_j/(\rho V_L^3)$.[15] Exploiting these relations, one can obtain from Eq. (27) that

$$F_D^2 = \frac{\pi^2 \Gamma^2 P_P P_S}{4\tilde{\Gamma}_0^2 \rho^2 V_L^6 f_P^4}. \tag{37}$$

Together with this, the left-hand side of Eq. (27a) gives

$$a_D^2(z) \ \Phi^{-2}(z, \delta, \xi) = \frac{P_D}{2\pi^2 \rho V_L f_D^2}. \tag{38}$$

Combining Eqs. (37) and (38), one can find the power density of the difference-frequency acoustic wave

$$P_D = 4\pi^2 P_P P_S m \left(\frac{f_D^2}{f_P^4}\right) \Phi^2(z, \delta, \xi), \tag{39a}$$

$$m = \frac{\pi^2 \Gamma^2}{8\rho \tilde{\Gamma}_0^2 V_L^5}. \tag{39b}$$

Now, one can estimate the total efficiency I of Bragg light scattering by the difference-frequency acoustic wave. In the particular case of rather weak acoustic signals, when nonlinearity inherent in acousto-optical interaction can be omitted,[15] one can use only a few terms from the corresponding expansion and write

$$I = \sin^2(qL) \approx q^2 L^2 - \frac{1}{3} q^4 L^4 + \cdots, \tag{40a}$$

$$q \approx \pi \lambda^{-1} \sqrt{M_2 P_D / 2}. \tag{40b}$$

Under natural condition $q^2 L^2 \ll 3$, i.e., under inequality

$$P_D \ll 6\lambda^2/(\pi^2 M_2 L^2), \tag{41}$$

one may restrict himself by the first term on the right-hand side of Eq. (40a) and rewrite Eq. (40a) as $I = \pi^2 M_2 L^2 P_D/(2\lambda^2)$. Sometimes [see, for instance, Eq. (44b)], it is worthwhile to exploit the parameter $\mu = (\pi^2/2) M_2 m$, which combines characterization of both nonlinear acoustic and linear acousto-optic properties of material under consideration. The magnitude of I determines the combined efficiency of the acousto-optical cell under consideration in terms of light scattering. This result makes it possible to characterize the contribution of acousto-optical interaction exploiting Eq. (40a) in the form of

$$I_{max} = \pi^2 M_2 L^2 P_{D\,max} / (2\lambda^2). \tag{42}$$

With a maximally allowed level $P_{D\,max} \approx 5 \times 10^5$ g/s^3 $= 0.05$ W/cm^2, obtained from Eq. (41), one can find $I_{max} \approx 0.3$. This estimation makes it possible to consider the above-chosen level of P_D as more or less tolerable for an upper limit in a KRS–5 single crystal under the aforementioned condition given by Eq. (41). An undoubted merit of this characterization consists of practically convenient direct proportionality between the efficiency I and the power density P_D.

After that, the contribution of acoustic wave mixing should be briefly analyzed. With this object in view, one can use Eqs. (25) and (26) for estimating the acoustic pump power density P_{P0} needed to reaching a preassigned peak level of the difference-frequency power density $P_{D\,max}$ at a given ratio $\alpha = P_S/P_{P0}$. From the start, it should be noted that a peak magnitude peculiar to the squared coordinate dependence $\Phi_m^2 [z_m(\delta, \xi), \delta, \xi, G] = [G/z_m(\delta, \xi)] \Phi^2 [z_m(\delta, \xi), \delta, \xi]$ in, for example, Eq. (32) can be estimated as $\Phi_m^2 [z_m(\delta, \xi), \delta, \xi, G] \approx 0.1$ with $G = 4$ (see Fig. 7). Consequently, one can find

$$P_{P0} = \frac{f_P}{2\pi \delta \Phi_m [z_m(\delta, \xi), \delta, \xi, G]} \sqrt{\frac{P_{D\,max}}{\alpha m}}. \tag{43}$$

Let us consider the particular example related to a KRS–5 single crystal. When the required magnitude of I_{max} is, for instance, equal to 3% (which is quite reasonable for the spectrum analysis in a small-signal linear regime), Eq. (42) gives $P_{D\,max} \approx 3.0 \times 10^4$ g/s^3 $= 0.003$ W/cm^2. Then, taking $m \approx 1.1 \times 10^{11}$ s/g, $\alpha = 0.1$, $G = 4$, $\delta = 0.15$, $\xi = 1.0$, and $f_P = 1.5$ GHz, one can estimate from Eq. (43) the needed value of the acoustic pump power density by $P_{P0} \leq 0.83 \times 10^7$ g/s^3 $= 0.83$ W/cm^2, which looks, practically, quite acceptable.

6 Proof-of-Principal Experimental Modeling

The obtained theoretical results related to the collinear acoustic wave heterodyning were examined experimentally via exploitation of the acousto-optic technique. The main focus was paid to the process of generating the difference-frequency acoustic wave and the effect of heterodyning by itself. At this step, one must say that the above-presented analytical calculations allow mathematically scaling the parameters exploited within the problem. By this we mean that a principal physical opportunity exists for experimental simulation of the desirable collinear interaction between high-frequency acoustic waves passing along the wave axes in anisotropic solid state through studying a perfectly equivalent process at low frequencies in isotropic media with acceptable characteristics, namely, parameters of acoustic nonlinearity, acoustic attenuation, and acoustic and acousto-optical figures of merit. In our particular case, one can perform experimental simulation of codirectional collinear acoustic wave heterodyning in a 1.5-GHz frequency range in the KRS–5 crystal through studying the same process in the acousto-optical cell exploiting the distillated water (H_2O) at frequencies of ~100 MHz. Analysis of Eq. (39) shows that, if the original parameter γ is saved during both the scaling and the

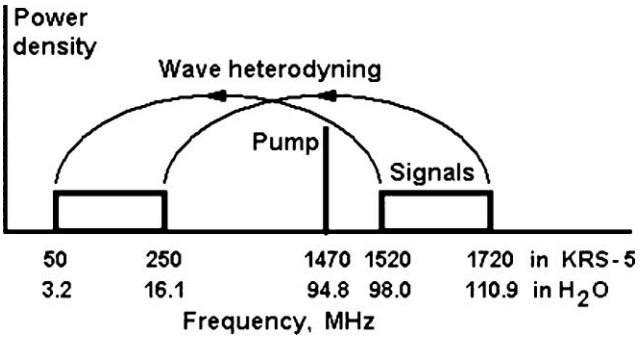

Fig. 11 General principle of the wave heterodyning and its experimental modeling.

experimental modeling, [i.e., $\gamma \equiv \gamma_M$ (where index M is related to the modeling process)], one can write

$$f_j^2 = \frac{\tilde{\Gamma}_{0,\,M}}{\tilde{\Gamma}_0}\, f_{j,\,M}^2, \tag{44a}$$

$$\frac{P_P P_S L^2}{\lambda^2} = \frac{\mu_M \tilde{\Gamma}_{0,\,M}}{\mu \tilde{\Gamma}_0}\, \left(\frac{P_{P,M} P_{S,M} L_M^2}{\lambda_M^2}\right). \tag{44b}$$

The index j in Eq. (44a) represents a generalization for all the indices exploited above. Taking into account the properties of water: $\rho_M = 1.0$ g/cm^3, $n_M = 1.33$, $|\Gamma_M| = 8$, $V_{L,M} = 1.49 \times 10^5$ cm/s, $\Gamma_{0,M} = 2400$ dB/(cm GHz^2), and $M_{2,M} = 126 \times 10^{-18}$ s^3/g, one can find $\tilde{\Gamma}_{0,M} \approx 5.52 \times 10^{-16}$ s^2/cm, $m_M \approx 3.53 \times 10^6$ s/g, and $\mu_M \approx 8.77 \times 10^{-9}$ s^4/(g cm). Using Eq. (44a), which gives the frequency factor $\sqrt{\tilde{\Gamma}_0/\tilde{\Gamma}_{0,M}} \cong 0.0645$, and utilizing the data from Sec. 4, which are related to Eq. (36) and illustrated by Fig. (8), one can calculate for the modeling medium (i.e., for the distilled water) that

$$f_{US,M} = 110.940\,\text{MHz}, \tag{45a}$$

$$f_{LS,M} = 98.045\,\text{MHz}, \tag{45b}$$

$$f_{P,M} = 94.815\,\text{MHz}, \tag{45c}$$

$$f_{DL,M} = 3.225\,\text{MHz}, \tag{45d}$$

$$f_{DU,M} = 16.125\,\text{MHz}. \tag{45e}$$

The general principle of the wave heterodyning and its experimental modeling are illustrated in Fig. 11. The obtained magnitudes of the operating frequencies for liquid cell keep a pair of the previously chosen parameters $\gamma_L \equiv \gamma_{L,M} = 1.034$ and $\gamma_U \equiv \gamma_{U,M} = 1.17$.

The frequency $f_{DU,M}$ from Eq. (45e) makes it possible to exploit the results of Sec. 4 for the modeling medium and to estimate potential clear aperture inherent in the water-based acousto-optical cell at a –3 dB level of acoustic losses along this aperture as $D_M \approx 5.0$ cm. Together with this, one has to estimate the Klein-Cool factor Q for the liquid cell. Taking, for example, $\lambda_M = \lambda = 671$ nm and $L_M = 2.5$ cm, one can estimate $Q \cong 0.4$ for $f_{DL,M} = 3.225$ MHz and $Q \cong 9.1$ for $f_{DU,M} = 16.125$ MHz. Thus, the Bragg region of light scattering could be expected for the acoustic difference frequencies, which are close to $f_{DU,M}$, while for the acoustic difference frequencies near $f_{DL,M}$ the transition region[8] of light scattering could be expected in this water-based cell. Nevertheless, both these options are acceptable for our purposes. In fact, they both give almost the same linear approximation, and this approximation alone is desirable within the small-signal linear regime of spectral data processing under consideration here.

In so doing, the experimental setup, whose optical part is presented in Fig. 12, has been arranged. The goals of our experiment did not touch the principal possibility of modeling the power-density relations, which are described by Eq. (44b). This fact is conditioned by really large technical difference in designing between a liquid-based acousto-optical cell and a solid state one. In our opinion, similar modeling cannot give adequate data being practically useful to help in creating the ultrahigh-frequency KRS–5 based cell. This is why at this step of modeling our attention was mainly concentrated on the physical principles of collinear acoustic wave heterodyning and the corresponding frequency relations.

Exploiting the above-listed estimations, the specific liquid-based acousto-optical cell of a new type had been designed and inserted in an almost standard optical scheme for acousto-optical spectrum analysis. This scheme includes a dark red-light laser ($\lambda_M = 671$ nm, the output optical power ~40 mW), a four-prism beam expander (only two of them are shown), a rectangular selecting optical diaphragm, a liquid-based acousto-optical cell with acoustic absorber and two radio-wave frequency electronic ports for the input signal and pump (see Fig. 13), a large-aperture achromatic doublet lens, and a 3000-pixel CCD linear array photocamera. A water-based liquid cell of ~6.0 cm in total length was lighted by the expanded optical beam being linearly polarized along the acoustic beam inside the cell. It provided, on the one

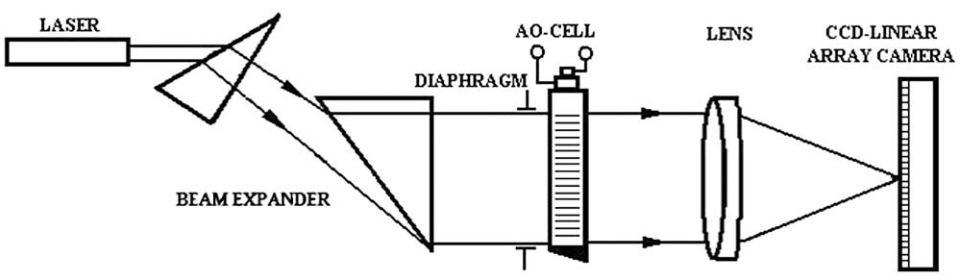

Fig. 12 Optical scheme for experimental acousto-optical modeling of the collinear wave heterodyning.

Fig. 13 Water-based liquid acousto-optical cell with acoustic absorber and two radio-wave frequency electronic ports.

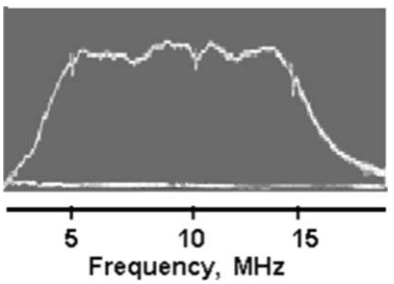

Fig. 14 The digitized oscilloscope trace reflecting the frequency distribution of the light intensity scattered by the acoustic wave with the difference frequency within the modeling experiment.

hand, the maximal transmission of the prism beam expander due to coinciding the plane of expanding laser beam with the corresponding vector of light polarization and, on the other hand, the maximal efficiency of acousto-optical interaction in water, because the effective photoelastic constant equals the maximum value $p_{11,M} = 0.274$. To underline the role of the cell within modeling, one should note that the same optical components and a multipixel CCD linear array photocamera could be practically used for operating over both the potential KRS–5–based cell and the water-based liquid cell. This opportunity is conditioned by rather similar sizes of their optical apertures, while a significant difference in their frequency performances will be reflected mainly in different angular alignments peculiar to the chosen Bragg regime of light scattering.

The piezoelectric transducer with an interaction length of 2.5 cm was made of a thin ($Y + 36$ deg)-cut lithium niobate crystal, so that it excited purely longitudinal acoustic wave at its resonant frequency close to $f_{0,M} \approx 103$ MHz and within the total frequency bandwidth of $\Delta f_M \geq 16$ MHz (i.e., 15.5%). The single-frequency pumping longitudinal acoustic wave with the power density of up to 0.6 mW/mm^2 was generated at the fixed carrier frequency of ~95 MHz, so that the case of $\gamma \in [1.04,\ 1.18]$ had been experimentally realized in frames of modeling. During the experiments, we placed a diaphragm in an ~8-mm vicinity of the piezoelectric transducers area (~13% of the total 6.0-cm aperture) to minimize the effect of this area, where an increase in the power of difference frequency waves takes place. Consequently, the available optical aperture of a cell was exceeding 5.0 cm. The efficiency of light scattering by longitudinal acoustic wave at the difference-frequency was slightly greater than 2%. Figure 14 shows the digitized oscilloscope trace of the light intensity distribution versus the difference frequency inherent in the resulting acoustic wave, which was generated in a water-based liquid cell realizing the algorithm of collinear wave heterodyning. This oscilloscope trace had been recorded by a multipixel CCD linear array photocamera through connecting the input signal port of a cell at the radio-wave sweep generator simulating the radio-wave signal. The scheme, connecting the sweep generator with the cell's piezoelectric transducer, included a two-section wideband matching circuit of the lumped components together with a two-cascade resistance step-down transformer assembled out of microcoaxial cables. The signal-like frequency was sweeping in the range of about 98–111 MHz, so that the difference frequency was varied in the range of about 3.0–16.5 MHz. It should be noted that for radio-wave signals, producing the dynamic acoustic gratings on the resulting carrier difference-frequencies of ~250 MHz in the KRS–5 crystal and ~16.2 MHz in the distilled water, the attenuation is close to a –3 dB level over the corresponding total cell apertures. At the same time, for the signal acoustic waves at even the lower original frequencies of ~1520 MHz in KRS–5 and ~98 MHz in water, the total attenuations exceed 110 dB along the corresponding apertures, which is perfectly unacceptable in practice.

7 Brief Comparative Discussion

The above-obtained results make it possible to perform theoretical estimations for potential number of parallel frequency channels and frequency resolution of spectrum analysis. Potential frequency resolution δf inherent in similar acousto-optical cell, operating in the regime of spectrum analysis, can be estimated from the following simple quantum mechanic consideration as $\delta f \approx V/D$. This value alone determines the physical limit of the frequency resolution peculiar to an acousto-optical cell, independently, on the number of phonons taking part in a process of the Bragg light scattering. Taking into account the above-listed values $V_L = 1.92 \times 10^5$ cm/s and $D = 5.0$ cm, one can find $\delta f \approx 38.4$ KHz. The number of parallel frequency channels for spectrum analysis can be calculated as $N = \Delta f / \delta f$. In the case of $\Delta f = 200$ MHz, one can obtain $N \approx 5210$. Moreover, because the initial frequencies under analysis are lying in the range 1520–1720 MHz, one can conclude that the relative accuracy of data processing can be estimated at least by the ratio $\delta f / f_0 \approx 2.37 \times 10^{-5}$. Then, the data from Sec. 4 show that, if the total efficiency of Bragg light scattering by the difference-frequency acoustic wave is chosen to be $I_0 = 0.03$ (i.e., 3%), one should provide $P_{P0} \leq 0.83 \times 10^7$ g/s^3 = 0.83 W/cm^2, and $P_S \leq 0.83 \times 10^6$ g/s^3 = 0.083 W/cm^2 due to $\alpha = 0.1$ with $L = 1.0$ cm (see Sec. 5).

At this step, it seems quite reasonable to compare operation characteristic of the proposed KRS–5 acousto-optical

cell with the corresponding characteristics of the traditional high-frequency cell. Perhaps, the best option for this purpose is connected with a crystalline cell exploiting longitudinal acoustic waves along the [100]-axis of uniquely low-loss lithium niobate ($LiNbO_3$) single crystal with $M_2 = 7.0 \times 10^{-18}$ s^3/g, $\Gamma = 0.15$ dB/(cm GHz^2), and $V_L = 6.57 \times 10^5$ cm/s. Each cell can be characterized in both frequency and amplitude domains. The best set of frequency characteristics for the chosen cell at the central frequency $f_0 = 1.6$ GHz (which is neighboring to the central frequency $f_0 = 1620$ MHz obtained for KRS–5 crystalline cell) includes the frequency bandwidth $\Delta f \approx f_0/2 = 810$ MHz, the upper signal frequency $f_U = 2.0$ GHz, the optical aperture $D_0 = 3[\text{dB}]/(\Gamma f_U^2) \approx 5.0$ cm associated with a 3-dB level of acoustic losses at the frequency f_U, the frequency resolution $\delta f = V/D_0 = 131.4$ KHz, the number of resolvable spots $N = \Delta f/\delta f \approx 6010$, and the relative accuracy of analysis $\delta f/f_0 \approx 8.2 \times 10^{-5}$. The efficiency of this cell with $L = 1.0$ cm and a given exciting acoustic wave power density P_0 can be estimated by $I_0 = \sin^2(q_0 L)$, where q_0 can be taken from Eq. (40b) at $\lambda = 671$ nm. To make the comparison to the data at the end of Sec. 2, let us take, as before, $I_0 = 0.03$ (i.e., 3%). In this case, one can estimate $q_0 = I^{1/2}/L \approx 0.173$ cm^{-1} and $P_0 = (2I\lambda^2)/(\pi^2 L^2 M_2) \approx 0.4 \times 10^7$ g/s^3 $= 0.4$ W/cm^2.

The above-mentioned data make it possible to conclude that the proposed KRS–5 based cell, exploiting the collinear acoustic wave heterodyning, provides increasing both the frequency resolution and the relative accuracy of analysis by ~3.4 times in comparison to the traditional lithium niobate cell. Together with this, the new KRS–5 cell ranks below the traditional lithium niobate cell in the number of resolvable spots by 13%. Then, to make the correct decision, one must take into account a few following circumstances. First, a large optical aperture requires growing a large-size boule of lithium niobate deprived of internal lattice defects. In fact, it should be the monodomained perfect single crystal exhibiting a high optical homogeneity and providing top-level conditions for propagation of both optical as well as UHF acoustic waves through a large-aperture cell. Practically, it is rather difficult to satisfy these requirements; otherwise, similar cells will have lost a significant part of its potential frequency resolution. Second, designing truly effective piezoelectric transducer with a 50% frequency bandwidth at a carrier frequency of ~1.6 GHz is not an ordinary task. The existing difficulties in technology of production as well as in subsequent acoustic and electronic matching of a similar wideband piezoelectric transducer can be resolved currently only by decreasing its efficiency or/and narrowing its bandwidth. This is why the above-noted potential frequency characteristics must be considered as only the limiting theoretical values. Third, the estimated efficiency for a lithium niobate cell cannot be applied directly to the comparison under consideration because the proposed new cell involves two cascades of processing and provides an additional function, namely, the heterodyning, which, naturally, needs additional power consumption.

8 Conclusion

The presented data demonstrate both the possibility and potential advantages of applying a codirectional collinear wave heterodyning to essential, about an order of magnitude or more, improvement of the frequency resolution within a multichannel parallel acousto-optical spectrum analysis of gigahertz-frequency range analog radio-wave signals. In so doing, we have theoretically investigated the phenomenon of a codirectional collinear wave heterodyning, taken in the particular case of mixing the longitudinal acoustic waves of finite amplitudes. Then, an opportunity of implementing acousto-optical data processing with the wave heterodyning has been experimentally modeled utilizing the specially designed acousto-optical cell based on distilled water. Together with this, the methods for estimating the total efficiency of operation and optimizing aperture parameters for the cell of a new type have been developed. The proposed technique exploits a two-cascade algorithm of processing and is intended for direct parallel and precise optical spectrum analysis and provides more then 5000 frequency channels for processing analog radio-wave signals in a gigahertz-frequency range with the accuracy or with the relative frequency resolution ~10^{-5}, which is usually unattainable for conventional direct acousto-optical methods. The obtained results reflect the fruitful character of modern approaches based on applying various nonlinear phenomena to improving the performance data of optical processing and give an appropriate example of this kind. A few practical advantages of the presented approach can be noted. First, the proposed device does not need additional electronic equipment for mixing the signals and selecting the resulting carrier frequency, because heterodyning can be performed directly in a cell and provides potentially the dynamic range of ~90 dB peculiar to wave processes in solids. Then, the approach under consideration decreases the required relative bandwidth of piezoelectric transducer from 50 to 100% at the resulting frequency within a conventional cell to 15% at the initial carrier frequency. Third, in the case of a spatially multichannel arrangement of the acousto-optical cell, the identity of neighboring spatial channels to each other can be provided by adjusting the corresponding heterodynes. Finally, one should note that the number of isotropic or crystalline materials, which are appropriate for acousto-optical cells processing signals in a gigahertz-frequency range, is definitely restricted due to fast-growing influence of square-law frequency dependence for the acoustic attenuation in solids. For instance, one can easily show that the above-discussed KRS–5 cubic crystal cannot be used for creating a conventional acousto-optical cell operating with signals whose carrier frequency exceeds about 400–500 MHz. Nevertheless, this crystalline material, alone, can be, in principle, exploited for the control over $f_0 = 1.6$ GHz signals. Consequently, one can conclude that a two-cascade arrangement of a cell presented here allows extending the spectrum of acousto-optical materials being appropriate for direct processing of ultrahigh-frequency analog radio-wave signals.

Acknowledgment

The work was financially supported by the CONACyT, Mexico (Project No. 61237).

References

1. Yu. S. Kivshar and G. P. Agrawal, *Optical Solitons: from Fibers to Photonic Crystals*, Academic Press, New York (2003).
2. N. N. Akhmediev and A. Ankiewich, *Solitons: Nonlinear Pulses and Beams*, Chapman & Hall, London (1997).

3. A. S. Shcherbakov and A. Aguirre Lopez, "Wave multiplication of binary encoded data exploiting solitary multi-pulse non-collinear three-wave coupled states," *J. Opt. A* **8**, 464–472 (2006).
4. A. S. Shcherbakov, A. M. Bliznetsov, A. L. Castellanos, and D. Sánchez Lucero, "Acousto-optical spectrum analysis of ultra-high frequency radio-wave analogue signals with an improved resolution exploiting the collinear acoustic wave heterodyning," *OPTIK–Int. J. Light Electron. Opt.* **121**, 1497–1506 (2010).
5. A. S. Shcherbakov, D. Sánchez Lucero, A. Luna Castellanos, and O. I. Belokurova, "Direct multi-channel optical spectrum analysis of radio-wave signals using collinear wave heterodyning in single acousto-optical cell," *J. Opt.* **12**(4), 045203 (2010).
6. P. A. M. Dirac, *The Principles of Quantum Mechanics*, 4th ed., Oxford University Press, London (1999).
7. Yu. E. Sirotin and M. P. Shaskol'skaya, *Fundamentals of Crystal Physics*, Mir Publ., Moscow (1982).
8. A. A. Blistanov. *Crystals for Quantum and Nonlinear Optics*, 2nd ed., MISIS, Moscow (2007).
9. V. G. Dmitriev, G. G. Gurzadyan, and D. N. Nikogosyan, *Handbook of Nonlinear Optical Crystals*, 3rd ed., Springer, Berlin (1999).
10. R. W. Klein and B. D. Cook, "A unified approach to ultrasonic light diffraction," *IEEE Trans. Sonics and Ultrasonics* **SU-14**(3), 123–134 (1967).
11. A. Norris, "Finite amplitude waves in solids," Chapter 9 in *Nonlinear Acoustics*, M. F. Hamilton and D. T. Blackstock, Eds., pp. 263–277 Academic Press, New York (1998).
12. V. V. Kludzin and V. V. Molotok, "Experimental characteristics of the elastic nonlinearity in KRS-5 and $NaBi(MoO_4)O_2$ crystals," in *1994 IEEE Ultrasonic Symp. Proc.* (Cannes, France), Vol. 2, pp. 851–854 (1994).
13. M. Abramovitz and I. A. Stegun, *Handbook of Mathematical Functions: with Formulas, Graphs, and Mathematical Tables*, Dover Publications, New York (1965).
14. G. A. Korn and T. M. Korn. *Mathematical Handbook for Scientists and Engineers*, 2nd. ed., McGraw-Hill, New York (1967).
15. A. Korpel, *Acousto-Optics*, Marcel-Dekker, New York (1997).

Biographies and photographs of the authors not available.